AGU PUBLICATIONS

Geophysical Research Letters

RESEARCH LETTER
10.1002/2017GL073323

Key Points:
- Silica-rich diagenetic halos penetrate lacustrine and unconformably draping aeolian bedrock in Gale crater, Mars
- Colocation of diagenetic and detrital silica suggests aqueous remobilization of detrital silica
- Presence of diagenetic halos in the unconformably draping aeolian bedrock suggests late-stage groundwater activity in Gale crater

Supporting Information:
- Supporting Information S1

Correspondence to:
J. Frydenvang,
jfrydenvang@snm.ku.dk

Citation:
Frydenvang, J., et al. (2017), Diagenetic silica enrichment and late-stage groundwater activity in Gale crater, Mars, *Geophys. Res. Lett.*, *44*, doi:10.1002/2017GL073323.

Received 2 MAR 2017
Accepted 24 APR 2017
Accepted article online 26 APR 2017
Corrected 30 MAY 2017

This article was corrected on 30 MAY 2017. See the end of the full text for details.

Diagenetic silica enrichment and late-stage groundwater activity in Gale crater, Mars

J. Frydenvang[1,2], P. J. Gasda[1], J. A. Hurowitz[3], J. P. Grotzinger[4], R. C. Wiens[1], H. E. Newsom[5], K. S. Edgett[6], J. Watkins[4], J. C. Bridges[7], S. Maurice[8], M. R. Fisk[9], J. R. Johnson[10], W. Rapin[4], N. T. Stein[4], S. M. Clegg[1], S. P. Schwenzer[11], C. C. Bedford[11], P. Edwards[7], N. Mangold[12], A. Cousin[8], R. B. Anderson[13], V. Payré[14], D. Vaniman[15], D. F. Blake[16], N. L. Lanza[1], S. Gupta[17], J. Van Beek[6], V. Sautter[18], P.-Y. Meslin[8], M. Rice[19], R. Milliken[20], R. Gellert[21], L. Thompson[22], B. C. Clark[23], D. Y. Sumner[24], A. A. Fraeman[25], K. M. Kinch[2], M. B. Madsen[2], I. G. Mitrofanov[26], I. Jun[25], F. Calef[25], and A. R. Vasavada[25]

[1]Los Alamos National Laboratory, Los Alamos, New Mexico, USA, [2]Faculty of Science, University of Copenhagen, Copenhagen, Denmark, [3]Department of Geosciences, Stony Brook University, Stony Brook, New York, USA, [4]Division of Geological and Planetary Sciences, California Institute of Technology, Pasadena, California, USA, [5]Department of Earth and Planetary Sciences, University of New Mexico, Albuquerque, New Mexico, USA, [6]Malin Space Science Systems, San Diego, California, USA, [7]Space Research Center, Department of Physics and Astronomy, University of Leicester, Leicester, UK, [8]L'Institut de Recherche en Astrophysique et Planétologie, Toulouse, France, [9]College of Earth, Ocean, and Atmospheric Sciences, Oregon State University, Corvallis, Oregon, USA, [10]Applied Physics Laboratory, The Johns Hopkins University, Laurel, Maryland, USA, [11]Department of Environment, Earth and Ecosystems, The Open University, Milton Keynes, UK, [12]Laboratoire de Planétologie and Géodynamique de Nantes, CNRS, Université de Nantes, Nantes, France, [13]United States Geological Survey, Flagstaff, Arizona, USA, [14]GeoRessources, Université de Lorraine, Nancy, France, [15]Planetary Science Institute, Tucson, Arizona, USA, [16]NASA Ames Research Center, Moffett Field, California, USA, [17]Department of Earth Science and Engineering, Imperial College London, London, UK, [18]IMPMC, Muséum National d'Histoire Naturelle, Paris, France, [19]Geology Department, Western Washington University, Bellingham, Washington, USA, [20]Department of Geological Sciences, Brown University, Providence, Rhode Island, USA, [21]Department of Physics, University of Guelph, Guelph, Ontario, Canada, [22]Department of Earth Sciences, University of New Brunswick, Fredericton, New Brunswick, Canada, [23]Space Science Institute, Boulder, Colorado, USA, [24]Earth and Planetary Sciences, University of California, Davis, California, USA, [25]Jet Propulsion Laboratory, California Institute of Technology, Pasadena, California, USA, [26]Space Research Institute, Moscow, Russia

Abstract Diagenetic silica enrichment in fracture-associated halos that crosscut lacustrine and unconformably overlying aeolian sedimentary bedrock is observed on the lower north slope of Aeolis Mons in Gale crater, Mars. The diagenetic silica enrichment is colocated with detrital silica enrichment observed in the lacustrine bedrock yet extends into a considerably younger, unconformably draping aeolian sandstone, implying that diagenetic silica enrichment postdates the detrital silica enrichment. A causal connection between the detrital and diagenetic silica enrichment implies that water was present in the subsurface of Gale crater long after deposition of the lacustrine sediments and that it mobilized detrital amorphous silica and precipitated it along fractures in the overlying bedrock. Although absolute timing is uncertain, the observed diagenesis likely represents some of the most recent groundwater activity in Gale crater and suggests that the timescale of potential habitability extended considerably beyond the time that the lacustrine sediments of Aeolis Mons were deposited.

1. Introduction

The Mars Science Laboratory (MSL) rover, Curiosity, landed in Gale crater, Mars, on 6 August 2012, to investigate past and present habitability. Aeolis Mons (informally Mount Sharp) is a 5 km high mountain of stratified rock that includes hematite-, phyllosilicate-, and sulfate-bearing stratigraphic layers [*Malin and Edgett*, 2000; *Milliken et al.*, 2010; *Fraeman et al.*, 2016]. Collectively, the strata in Mount Sharp, below an apparent topmost anhydrous stratal package, are referred to as the Mount Sharp group [*Grotzinger et al.*, 2015; *Fraeman et al.*, 2016]. Curiosity's investigations indicate that Gale had an ancient habitable environment and that layers of the Mount Sharp group were deposited in a series of long-lived lakes dating into the Hesperian era [*Grotzinger et al.*, 2013; *Williams et al.*, 2013; *Grotzinger et al.*, 2015]. After deposition of the Mount Sharp group, it is thought that Gale crater experienced one or more episodes of burial and erosion to create the modern geomorphology [*Grotzinger et al.*, 2015; *Fraeman et al.*, 2016; *Watkins et al.*, 2016].

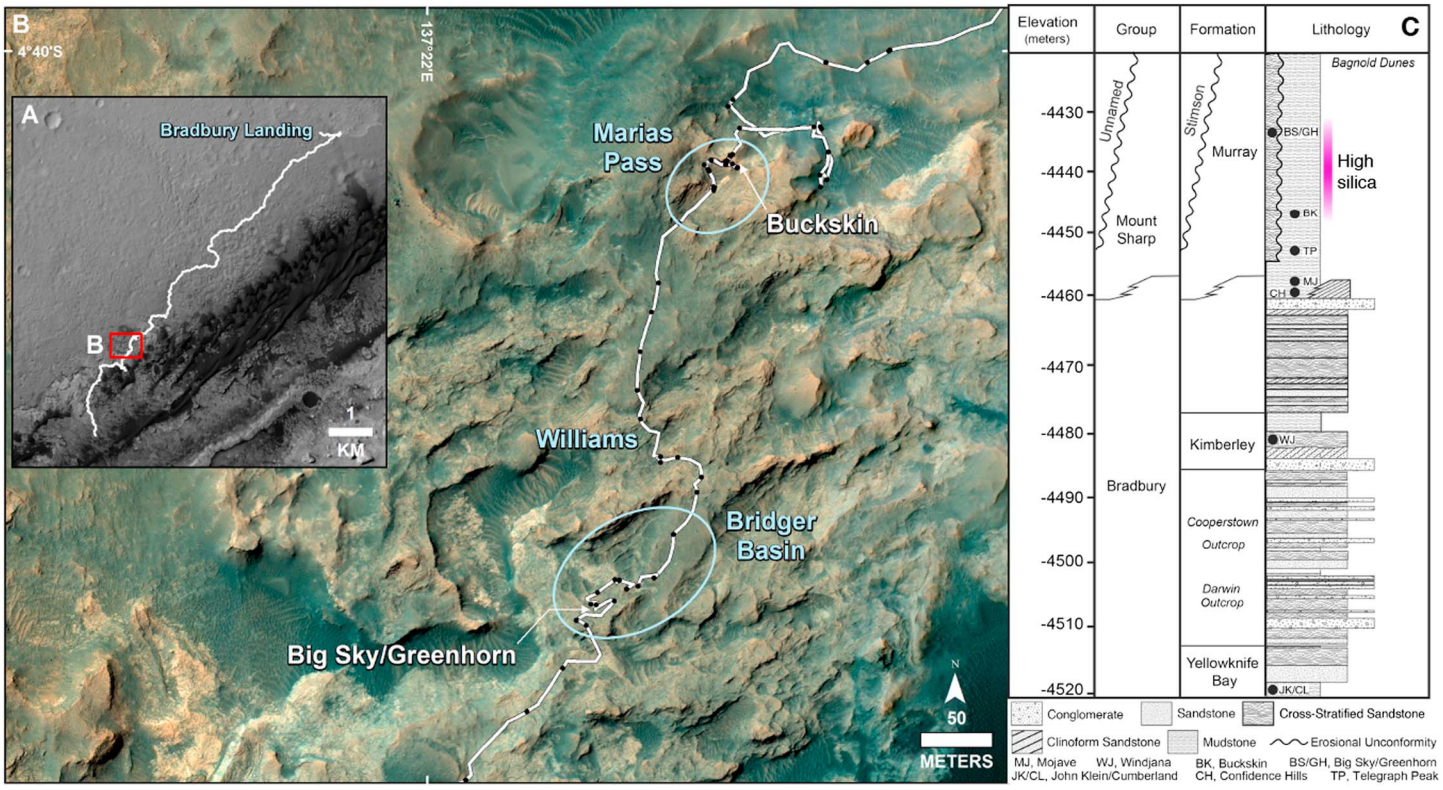

Figure 1. Study area: (a) Curiosity's traverse (white line) from the August 2012 landing site to the rover's position in December 2016; (b) Mars Reconnaissance Orbiter High-Resolution Imaging Science Experiment image mosaic from *Calef and Parker* [2016] showing the study area. The region traversed between Marias Pass and Bridger Basin is referred to as Williams. Each black dot represents an end-of-drive location, and the locations of the Buckskin, Big Sky, and Greenhorn drill sites are noted. (c) Stratigraphic column showing the lowermost encountered Mount Sharp group rocks with the unconformably overlying Stimson formation. The approximate elevation range of the observed detrital and diagenetic silica enrichment is highlighted.

Here we present the observation of silica-rich diagenetic features that crosscut lacustrine mudstone beds of the Mount Sharp group and younger, superimposed aeolian bedrock. These are colocated with previously reported detrital silica enrichment [*Morris et al.*, 2016]. Based on composition measurements by Curiosity's Chemistry and Camera (ChemCam) instrument [*Maurice et al.*, 2012; *Wiens et al.*, 2012], Alpha-Particle X-ray Spectrometer (APXS) [*Campbell et al.*, 2012; *Gellert et al.*, 2015], and cameras [*Edgett et al.*, 2012; *Maki et al.*, 2012; *Malin et al.*, 2010], we show that precipitation of amorphous silica sourced from the migration of late-stage groundwater through silica-rich bedrock provides a causal explanation for the colocated detrital and diagenetic silica.

2. Setting

Gale is a 155 km diameter impact crater that formed in the late Noachian or early Hesperian era [*Thomson et al.*, 2011], located at the martian dichotomy boundary at 4.6°S, 137.4°E. The Curiosity rover landed on Aeolis Palus, an alluvial plain in northern Gale. The rover's traverse has taken it onto the lower exposures of the Mount Sharp group, where elevated silica observations were first made in the lacustrine Murray formation on Mars solar day (sol) 991 of the mission. For the following ~200 sols, Curiosity investigated the nature of high-silica bedrock over a ~300 m traverse between Marias Pass and Bridger Basin in both the Murray formation and the unconformably overlying aeolian sandstones of the Stimson formation (Figure 1). High-silica Stimson formation was observed again ~120 sols later in the mission, ~350 m farther west at a similar elevation. The Stimson formation outcrop at that location, the Naukluft Plateau, is similar to what is described here but lacks exposure of underlying Murray formation.

The Murray formation is a lacustrine mudstone exhibiting mostly fine scale laminations; it represents the stratigraphically lowermost exposed unit of the Mount Sharp group [*Grotzinger et al.*, 2015]. The Stimson formation is a crossbedded aeolian sandstone facies that unconformably drapes Murray formation bedrock and

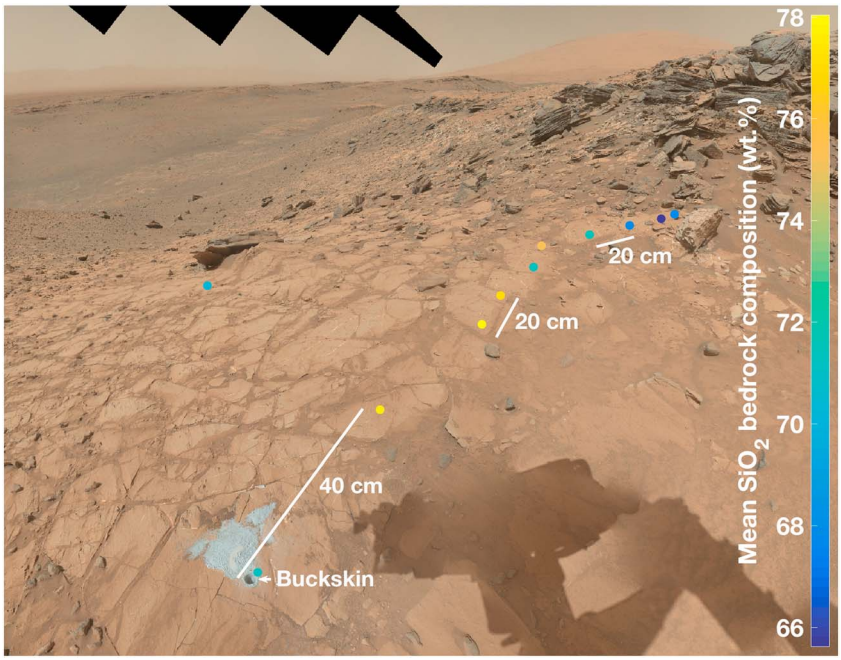

Figure 2. Marias Pass observations: Mars Hand Lens Imager mosaic acquired on sol 1065. View is toward the southeast, and the summit of Aeolis Mons (Mount Sharp) is observed in the background. Colored dots represent the locations of ChemCam Murray formation observations; colors indicate the mean bedrock silica content. The dark-toned bedrock and loose cobbles at the upper right are Stimson formation rocks.

is interpreted to postdate the burial and subsequent exhumation and erosion of the Mount Sharp group [*Fraeman et al.*, 2016; *Banham et al.*, 2017; *Watkins et al.*, 2016]. Exposures of the Murray formation are evident at erosional windows at Marias Pass (elevation −4448 m relative to the martian datum) and Bridger Basin (−4434 m); only the Stimson formation was exposed along the traverse between these locations (an area collectively referred to, here, as Williams).

3. Observations

Large chemical variations are observed in the Murray formation at Marias Pass, but these are generally not visually apparent (Figure 2). Only the lowest silica occurrences of the Murray formation (~57 wt % SiO_2) are noticeably darker than higher-silica occurrences [*Johnson et al.*, 2015] (supporting information Figure S1). The Buckskin drill sample was extracted on sol 1060 from an occurrence of high-silica Murray formation at Marias Pass (Figure 2). *Morris et al.* [2016] reported that the Buckskin sample consists of ~60% amorphous and ~40% crystalline material. Notably, monoclinic tridymite, a SiO_2 polymorph, constitutes ~34 wt % of the crystalline mineralogy, while amorphous silica dominates the amorphous component (~77 wt % SiO_2). As *Morris et al.* [2016] interpret the tridymite as detrital in origin, the Buckskin sample is consistent with previous analyses that show no evidence of high-temperature (>80°C) diagenesis in Gale [*Vaniman et al.*, 2014; *Bridges et al.*, 2015; *Rapin et al.*, 2016].

The Stimson formation generally displays a homogeneous composition and appearance, but elevated silica was measured in a lighter-toned lens in the Stimson formation at a contact between the Murray and Stimson formations at Marias Pass [*Newsom et al.*, 2016]. Furthermore, light-toned, fracture-associated halos that crosscut bedding were observed in the Stimson formation at Marias Pass, Williams, and Bridger Basin (Figure 3 and supporting information Figure S2). Where measured, the halos consistently had elevated silica. Two drill samples, Greenhorn and Big_Sky, were extracted, respectively, from within and outside a Stimson formation halo at Bridger Basin (Figure 3). Analysis by the Chemistry and Mineralogy (CheMin) instrument revealed a >40% increase in X-ray amorphous material, largely as amorphous silica, in Greenhorn relative to Big Sky, and an increased feldspar to pyroxene ratio [*Yen et al.*, 2017]. Similar to the results from the Buckskin sample, no evidence of high-temperature diagenetic minerals were observed [*Yen et al.*, 2017].

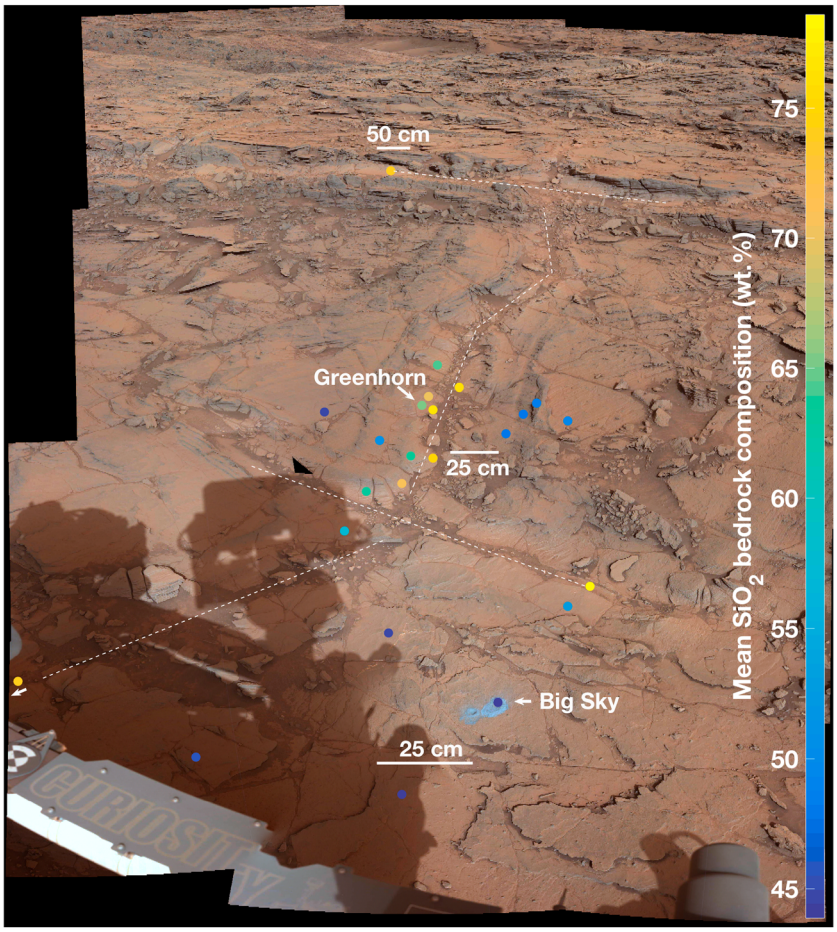

Figure 3. Bridger Basin observations: Mastcam-34 mosaic of the Big Sky and Greenhorn drill sites. The Big Sky sample was collected from outside, and the Greenhorn sample from inside, a fracture-associated halo in the Stimson formation. The ChemCam observations of the mean bedrock silica content are indicated by color-coded dots. Dashed lines indicate the approximate centerlines of the fracture-associated halos. Images were acquired on sols 1112, 1119, and 1126 (sequences mcam04954, mcam04956, mcam04986, and mcam05017).

At Bridger Basin, the Murray formation is exposed in two erosional windows, separated by ~2 m of elevation. The higher elevation site contains an outcrop of Murray formation comparable to exposures investigated south of Bridger Basin. In contrast, the lower elevation site displays light-toned fracture-associated halos that crosscut bedding, similar to those observed in the Stimson formation (supporting information Figure S3). Furthermore, halos can be tracked from the underlying Murray formation and into the Stimson formation (supporting information Figure S4), suggesting a common origin that postdates burial and lithification of the Stimson formation. The difference in tone between the lighter-toned halos and darker-toned bedrock is comparable, though slightly darker overall, to the difference in tone observed at Marias Pass between the highest and lowest silica Murray formation outcrops (supporting information Figure S1).

Ca-sulfate veins are ubiquitous in the Murray formation at both Marias Pass and Bridger Basin but are only occasionally observed in the Stimson formation outside fracture-associated halos. Within high-silica Stimson formation occurrences, Ca-sulfate was observed consistently as either well-defined veins (supporting information Figure S5) or as apparent intergranular cement [*Newsom et al.*, 2016].

4. Major and Minor Element Content

The Murray formation mudstone at Marias Pass and Bridger Basin is enriched in silica relative to Murray formation occurrences observed at lower and higher elevations (supporting information Figure S6). Excluding the highest elevation Murray formation outcrop analyzed at Bridger Basin, ChemCam observations indicate

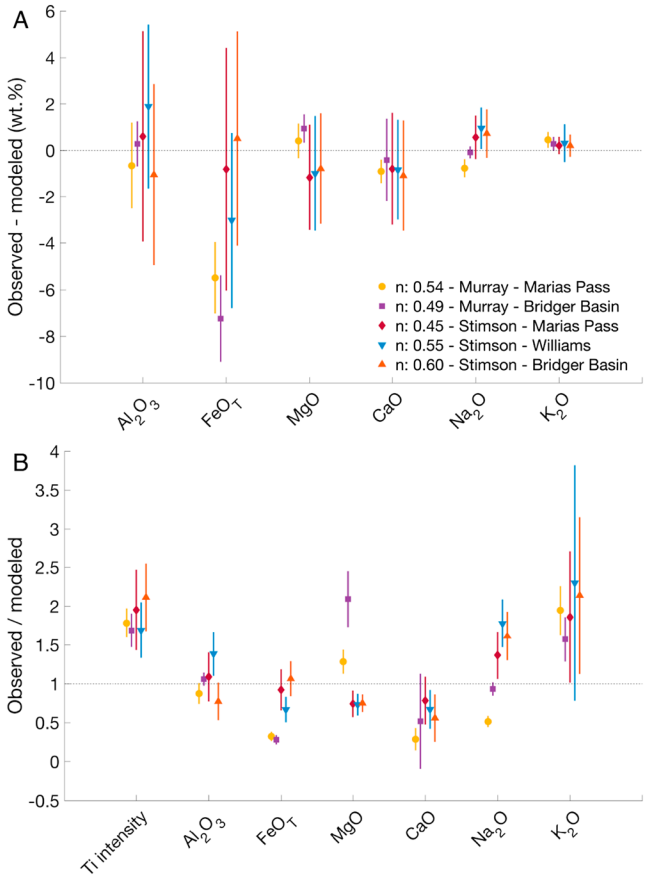

Figure 4. Dilution model based on ChemCam data: (a) Absolute difference in elemental composition between the ChemCam observed high-silica composition, and the dilution model output for addition of pure silica to low-silica targets, in both the Murray and Stimson formations at the indicated locations. The proportion of silica added is noted by "n." (b) Relative difference between the measured high-Si composition and the calculated dilution model output.

silica contents ranging between ~60 wt % and ~80 wt % at these locations. Increased silica does not appear to be associated with contacts between the Murray and Stimson formations (Figure 2).

Outside light-toned halos, the Stimson formation has an average of ~45 wt % SiO_2. Inside the halos, ChemCam observes >80 wt % SiO_2 closest to the centers of the halos, with silica content decreasing at centimeter scale radial to the halo centerlines (Figure 3 and supporting information Figure S4).

Owing primarily to differences in areal coverage and target placement, the ChemCam and APXS measurements differ somewhat (see supporting information Text S1) but agree overall on compositional trends (supporting information Figure S7). Both APXS and ChemCam observations show a decrease in FeO_T and Al_2O_3 with increasing silica in both the Murray and Stimson formations, although APXS generally measures lower Al and Fe content relative to colocated ChemCam measurements. ChemCam also shows decreasing CaO in both the Murray and Stimson formations with increasing silica. APXS, on the other hand, shows invariant CaO in elevated silica sites in the Stimson formation, and APXS CaO concentrations are generally higher than in the colocated ChemCam observations. The concentration of Na_2O is variable but tends to generally decrease in abundance with increasing SiO_2—most noticeably in the Murray formation. K_2O does not vary with silica in the Murray formation, averaging ~1 wt%. K_2O is at the level of ChemCam quantification in the Stimson formation (~0.3 wt %). MgO content appears to be at the ChemCam level of quantification (~2 wt %) for all Murray formation targets, whereas the Stimson formation shows a decrease from ~8 wt % to ~2 wt % with increasing silica. For APXS, a large decrease is also observed for Mg with increasing silica; low Mg is especially evident in APXS measurements of drill cuttings and fines.

The standard ChemCam TiO_2 calibration [*Wiens et al.*, 2013; *Clegg et al.*, 2017] performs suboptimally for high-silica compositions (see supporting information Text S2). Instead, the nonnormalized intensity of three diagnostic Ti spectral lines is used as a qualitative measure of ChemCam Ti content. The Ti content remains approximately constant with increasing SiO_2 within individual groups (supporting information Figure S8), but notably, the Murray formation at Marias Pass has higher TiO_2 content relative to other locations. As observations of drill fines provide the least interference from dust or sample inhomogeneity for APXS, it is particularly noteworthy that the Ti content does not change markedly between the Big Sky and Greenhorn drill fines, indicating that the process of silica enrichment in the fracture-associated halo at this location did not dramatically alter the concentration of Ti.

APXS also quantifies the elements S, P, Cl, Cr, Mn, Ni, Zn, and Br. Besides S and P, these elements generally decrease with increasing silica (supporting information Figure S9). SO_3 is observed to increase with increasing silica in the Stimson formation and remains approximately constant in the Murray formation. P_2O_5 is observed to increase with increasing silica in the Stimson formation and to a lesser degree in the Murray formation.

The large number of ChemCam observations allows definition of high- and low-silica compositions for the Murray and Stimson formations at different locations. (See supporting information section 1.) These end-member compositions enable modeling the effects of dilution, by silica, on the bulk composition of low-silica Murray or Stimson formation targets and examination to see if this model matches the observed bulk composition of high-silica Murray or Stimson formation targets (Figure 4).

Across the five groups (Murray formation at Marias Pass and Bridger Basin; Stimson formation at Marias Pass, Williams, and Bridger Basin), 45–60 vol % of silica addition is needed to account for the observed increase in silica (Figure 4). Comparing absolute differences between observed and modeled compositions (Figure 4a), good agreement is generally observed, but the low iron content observed in high-silica Murray formation is not well explained by a pure silica dilution model. From the standpoint of relative differences (Figure 4b), the dilution model also cannot explain the constant K_2O abundance in the Murray formation nor the constant TiO_2 across all groups. As MgO and K_2O are at the level of quantification even in the low-silica targets in the Murray and Stimson formations, respectively, any expected decrease cannot be observed by ChemCam.

5. Discussion

The presence of silica-rich fracture-associated halos crosscutting bedding in both the Murray and Stimson formations implies that the halos are diagenetic and that the silica enrichment postdates the deposition and lithification of the aeolian Stimson formation. The diagenetic silica enrichment therefore substantially postdates cessation of the lacustrine activity recorded by the Mount Sharp group. The elevated silica observed in the Murray formation at Marias Pass is likely both detrital and diagenetic. *Morris et al.* [2016] concluded that the tridymite observed in the Buckskin sample has a silicic volcanic provenance and was transported to Gale during the accumulation of the Murray formation. Given this provenance, considerable amounts of amorphous silica may have been transported and deposited with the tridymite or have been precipitated as authigenic sediment from the lacustrine water column due to the influx silicic volcanic material [*Hurowitz et al.*, 2017]. This would result in an initial detrital crystalline and amorphous silica enrichment. However, the presence of halos and observations of elevated silica in the Stimson formation at Marias Pass suggest that this area was also affected by the later diagenesis.

Under low-pH conditions, silica phases are generally less soluble than other minerals, thereby leading to a passive enrichment of silica [*McAdam et al.*, 2008]. Furthermore, active silica enrichment can occur as a result of silica precipitation, either due to a decrease in pH from an alkaline condition or from a drop in temperature as silica solubility is strongly dependent upon fluid temperature [*Williams and Crerar*, 1985; *Dove and Rimstidt*, 1994]. Both passive and active silica enrichments are commonly observed in geothermal systems, depending on their character, and have been invoked to explain in situ discoveries of silica-rich materials on Mars at the Mars Exploration Rover *Spirit* site in Gusev crater [*Squyres et al.*, 2008; *Ruff and Farmer*, 2016]. As stated previously, however, no evidence of high-temperature mineral phases that might indicate a hydrothermal environment have been observed in Gale crater. Accordingly, more relevant analogues to the observed silica enrichment may be found in the silica cements that are ubiquitous in clastic sedimentary rocks on Earth, where cements are generally associated with lower temperature ($<$80°C) formation conditions [e.g., *McBride*, 1989; *Vagle et al.*, 1994; *Thiry et al.*, 2015]. Typically, Earth silica cements are made of quartz, but diagenetic conditions at Gale crater were apparently inappropriate to the maturation of the observed amorphous products to a more stable quartz phase. Also, early in Earth's history, silica accumulated as authigenic sediment in iron formations [*Fischer and Knoll*, 2009] and in silicilyte deposits [*Ramseyer et al.*, 2013].

For the acquired Murray and Stimson bedrock observations, a preferential leaching of Ca, Na, and K relative to Al is not observed (Figure 4) as would be expected if the differences between high- and low-silica bedrock resulted from leaching during chemical weathering [*Hurowitz et al.*, 2005]. The absence of jarosite [*Yen*

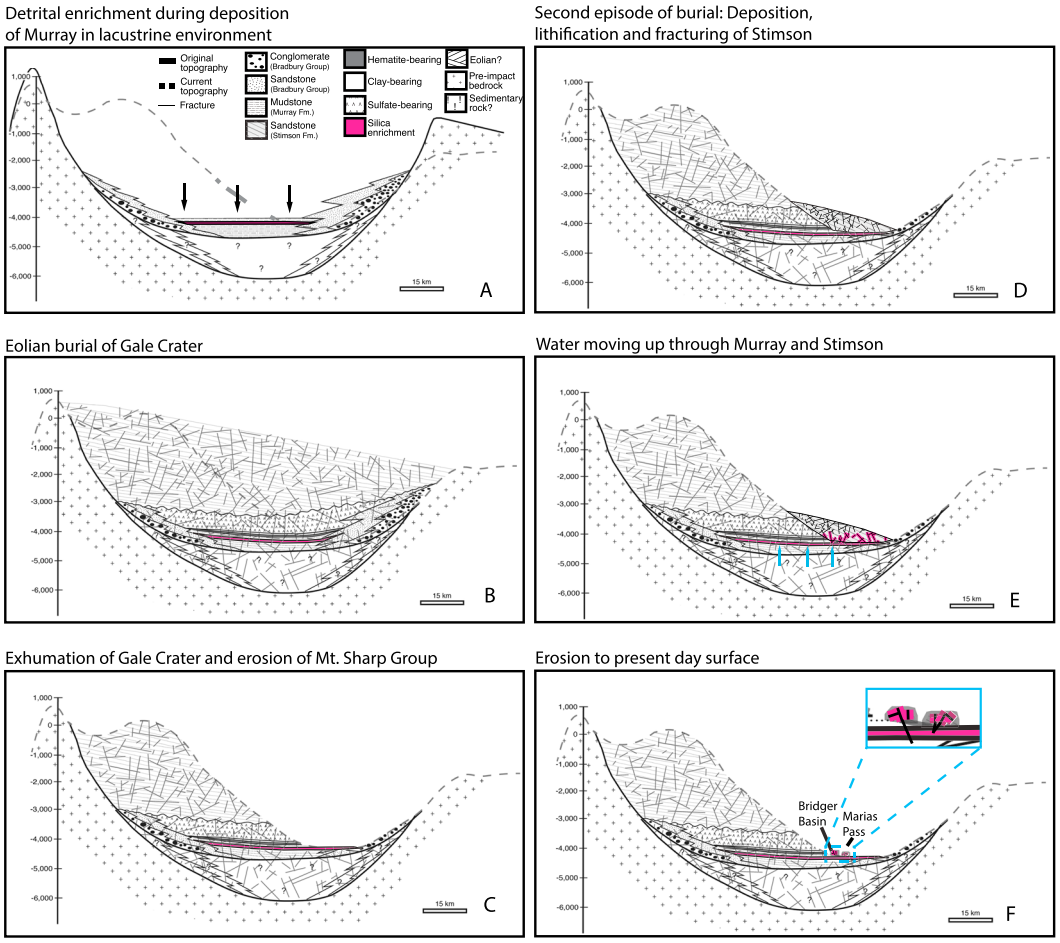

Figure 5. Proposed sequence of events: Hypothesized chronological sequence explaining the observed colocated detrital and diagenetic silica enrichment. The degree of aeolian burial is shown only to serve as illustrations. The dashed black line represents the approximate modern day geomorphology of Gale.

et al., 2017] and other low-pH indicator minerals indicates that a strong acid leaching environment is not the cause for this lack of preferential leaching [*Hurowitz et al.*, 2006; *Markússon and Stefánsson*, 2011]. Dilution with pure silica provides a reasonable representation of the content of multiple elements relative to the observed bedrock content (Figure 4). Likewise, the calculated addition of silica to account for its increase is consistent with the increase in the amorphous component (>40%) between the Big Sky and Greenhorn drill samples [*Yen et al.*, 2017]. However, a dilution with pure silica cannot account for the full drop in Fe observed in the Murray bedrock (Figure 4). The apparent constant Ti and constant K in Murray specifically, as well as the positive correlation of P and Si (supporting information Figures S7–S9), do not fit with either leaching or pure silica precipitation.

A more complex model that, for example, accounts for the expected preferential dissolution of pyroxene relative to feldspar [*Stefánsson et al.*, 2001], consistent with the observed differences between the Greenhorn and Buckskin samples [*Yen et al.*, 2017], would enable better modeling of the observed composition from the additional variables alone. However, the observed bedrock composition and ubiquity of Ca-sulfate veins rather suggest that multiple fluid events interacted with the bedrock in addition to the formation of the high-silica halos. Such additional fluid events imply that the positive correlation between Si and P could be purely coincidental and thus confounds the ability to sufficiently constrain the additional variables in a more complex model. Furthermore, inclusion of Ca-sulfate within the APXS field of view likely explains the correlation between SiO_2 and SO_3 and constant CaO observed by APXS in Stimson bedrock and likely also causes the lower content of Fe and Al measured by APXS relative to ChemCam. The difference in Mg measured by APXS

between drill fines and surface targets is likely due to the very short APXS penetration depth for Mg [*Rieder et al.*, 2003], resulting in a greater effect of even a slight dust coating (see supporting information Text S1).

While a perfect match between modeled and observed bedrock compositions remains elusive, the colocation of the detrital silica enrichment observed in the Buckskin sample and the diagenetic silica enrichment observed in halos (Figure 1c) provides clues to the likely diagenetic story. If the diagenetic silica enrichment was the result of leaching of other elements, then the observed colocation of detrital and diagenetic silica enrichment, separated by a substantial period of time, would be entirely coincidental. Rather, the detrital enrichment in amorphous silica could form a source for a subsequent active silica enrichment, thus providing a causal explanation for the colocation. As the observed high-silica composition is consistent with the primary source of the silica enrichment being precipitation of amorphous silica, this is considered the most parsimonious hypothesis.

Building on the sequence of events presented by *Grotzinger et al.* [2015], we propose the following augmentation to explain the colocated detrital and diagenetic silica enrichment. During deposition of the Mount Sharp group, silicic volcanic material, including tridymite [*Morris et al.*, 2016], was transported into the ancient Gale crater lake and deposited, along with amorphous silica, in the Murray strata observed at Marias Pass (Figure 5a). Overlying layers of the Mount Sharp group accumulated and following the cessation of Mount Sharp group lacustrine activity, the sediments were buried (Figure 5b). Subsequently, the Mount Sharp group was exhumed and eroded, thereby exposing Murray bedrock at an erosional surface comparable to the modern-day slope [*Watkins et al.*, 2016] (Figure 5c). Deposition and lithification of the Stimson formation followed (Figure 5d). During this second burial episode, we hypothesize that under pressure, neutral to alkaline groundwater moved upward through the Murray and Stimson formations along fractures that penetrated both units. As the groundwater encountered the silica-enriched Murray mudstones, silica was mobilized and carried into stratigraphically overlying Murray and Stimson rocks. There, changes in pH and/or temperature caused precipitation of the dissolved silica as opaline silica in zones parallel to the fractures through which the water moved (Figure 5e). Subsequent exhumation and ongoing erosion exposed the diagenetic halos currently observed at the surface (Figure 5f).

As Gale crater appears to have been buried, exhumed, and substantially eroded during the time elapsed between the accumulation of the Mount Sharp group and the subsequent deposition of the Stimson formation, the Stimson likely significantly postdates the Mount Sharp group [*Grotzinger et al.*, 2015; *Watkins et al.*, 2016]. Hence, this sequence of events implies that considerable amounts of neutral to alkaline groundwater were active in Gale crater well after Mount Sharp group lacustrine activity ceased [*Grotzinger et al.*, 2013, 2015]. Consequently, the timescale for potential habitability, at least in the subsurface of Gale, must be substantially extended.

Acknowledgments

This research was supported by the NASA MSL Mission, operated by the Jet Propulsion Laboratory, California Institute of Technology. We acknowledge the support of the MSL engineering and operations staff. J.F. thanks the Villum Foundation, and B.L. Ehlmann for help with data collection and early discussions of interpretation, K.M.K. and M.B.M. thank the Danish Council for Independent Research (4002-00292), J.C.B. and S.P.S. thank UKSA (ST/P002110/1), and C.C.B. thanks STFC (ST/N50421X/1) for support. Data from the MSL mission are available online (http://pds-geosciences.wustl.edu/missions/msl/). ChemCam and APXS derived data products used in this work are attached as supporting information.

References

Banham, S. G., et al. (2017), The Stimson formation: Determining the morphology of a dry aeolian dune system and its significance in Gale crater, Mars, *48th Lunar and Planetary Science Conference*, *48*, 2014.

Bridges, J. C., S. P. Schwenzer, R. Léveillé, F. Westall, R. C. Wiens, N. Mangold, T. Bristow, P. Edwards, and G. Berger (2015), Diagenesis and clay mineral formation at Gale crater, Mars, *J. Geophys. Res. Planets*, *120*, 1–19, doi:10.1002/2014JE004757.

Calef, F., III, and T. Parker (2016), MSL Gale merged orthophoto mosaic, PDS Annex, U.S. Geological Survey.

Campbell, J. L., G. M. Perrett, R. Gellert, S. M. Andrushenko, N. I. Boyd, J. A. Maxwell, P. L. King, and C. D. M. Schofield (2012), Calibration of the Mars science laboratory alpha particle X-ray spectrometer, *Space Sci. Rev.*, *170*(1–4), 319–340, doi:10.1007/s11214-012-9873-5.

Clegg, S. M., R. C. Wiens, R. Anderson, and O. Forni (2017), Recalibration of the Mars science laboratory ChemCam instrument with an expanded geochemical database, *Spectrochim. Acta B-Atom. Spectros.*, *129*, 64–85, doi:10.1016/j.sab.2016.12.003.

Dove, P. M., and J. D. Rimstidt (1994), Silica-water interactions, *Silica Phys. Behav. Geochem. Mater. Appl.*, *29*, 259–308.

Edgett, K. S., et al. (2012), Curiosity's Mars Hand Lens Imager (MAHLI) investigation, *Space Sci. Rev.*, *170*(1), 259–317, doi:10.1007/s11214-012-9910-4.

Fischer, W. W., and A. H. Knoll (2009), An iron shuttle for deepwater silica in late Archean and early Paleoproterozoic iron formation, *Geol. Soc. Am. Bull.*, *121*(1–2), 222–235, doi:10.1130/B26328.1.

Fraeman, A. A., B. L. Ehlmann, R. E. Arvidson, C. S. Edwards, J. P. Grotzinger, R. E. Milliken, D. P. Quinn, and M. S. Rice (2016), The stratigraphy and evolution of lower Mount Sharp from spectral, morphological, and thermophysical orbital data sets, *J. Geophys. Res. Planets*, *121*, 1713–1736, doi:10.1002/2016JE005095.

Gellert, R., B. C. I. Clark, and M. M. S. Teams (2015), In situ compositional measurements of rocks and soils with the alpha particle X-ray spectrometer on Nasa's Mars Rovers, *Elements*, *11*(1), 39–44, doi:10.2113/gselements.11.1.39.

Grotzinger, J. P., et al. (2013), A habitable fluvio-lacustrine environment at Yellowknife Bay, Gale crater, Mars, *Science*, *343*(6169), 1242777, doi:10.1126/science.1242777.

Grotzinger, J. P., et al. (2015), Deposition, exhumation, and paleoclimate of an ancient lake deposit, Gale crater, Mars, *Science*, *350*(6257), doi:10.1126/science.aac7575.

Hurowitz, J. A., S. M. McLennan, D. H. Lindsley, and M. Schoonen (2005), Experimental epithermal alteration of synthetic Los Angeles meteorite: Implications for the origin of Martian soils and identification of hydrothermal sites on Mars, *J. Geophys. Res.*, *110*, E07002, doi:10.1029/2004JE002391.

Hurowitz, J. A., S. M. McLennan, N. J. Tosca, R. E. Arvidson, J. R. Michalski, D. W. Ming, C. Schröder, and S. W. Squyres (2006), In situ and experimental evidence for acidic weathering of rocks and soils on Mars, *J. Geophys. Res.*, *111*, E02S19, doi:10.1029/2005JE002515.

Hurowitz, J. A., et al. (2017), Redox stratification of an ancient lake in Gale crater, Mars, *Science*, doi:10.1126/science.aah6849, in press.

Johnson, J. R., et al. (2015), ChemCam passive reflectance spectroscopy of surface materials at the Curiosity landing site, Mars, *Icarus*, *249*, 74–92, doi:10.1016/j.icarus.2014.02.028.

Maki, J., D. Thiessen, A. Pourangi, P. Kobzeff, T. Litwin, L. Scherr, S. Elliott, A. Dingizian, and M. Maimone (2012), The Mars science laboratory engineering cameras, *Space Sci. Rev.*, *170*(1), 77–93, doi:10.1007/s11214-012-9882-4.

Malin, M. C., and K. S. Edgett (2000), Sedimentary rocks of early Mars, *Science*, *290*(5), 1927–1937, doi:10.1126/science.290.5498.1927.

Malin, M. C., et al. (2010), The Mars Science Laboratory (MSL) Mast-mounted cameras (Mastcams) flight instruments, *41st Lunar and Planetary Science Conference, 41*, p. 1123.

Markússon, S. H., and A. Stefánsson (2011), Geothermal surface alteration of basalts, Krýsuvík Iceland—Alteration mineralogy, water chemistry and the effects of acid supply on the alteration process, *J. Volcanol. Geotherm. Res.*, *206*(1–2), 46–59, doi:10.1016/j.jvolgeores.2011.05.007.

Maurice, S., et al. (2012), The ChemCam instrument suite on the Mars Science Laboratory (MSL) rover: Science objectives and mast unit description, *Space Sci. Rev.*, *170*(1–4), 95–166, doi:10.1007/s11214-012-9912-2.

McAdam, A. C., M. Y. Zolotov, M. V. Mironenko, and T. G. Sharp (2008), Formation of silica by low-temperature acid alteration of Martian rocks: Physical-chemical constraints, *J. Geophys. Res.*, *113*, E08003, doi:10.1029/2007JE003056.

McBride, E. F. (1989), Quartz cement in sandstones: A review, *Earth Sci. Rev.*, *26*(1–3), 69–112, doi:10.1016/0012-8252(89)90019-6.

Milliken, R. E., J. P. Grotzinger, and B. J. Thomson (2010), Paleoclimate of Mars as captured by the stratigraphic record in Gale crater, *Geophys. Res. Lett.*, *37*, L04201, doi:10.1029/2009GL041870.

Morris, R. V., et al. (2016), Silicic volcanism on Mars evidenced by tridymite in high-SiO_2 sedimentary rock at Gale crater, *Proc. Natl. Acad. Sci. U.S.A.*, *113*(26), 7071–7076, doi:10.1073/pnas.1607098113.

Newsom, H. E., et al. (2016), The materials at an unconformity between the Murray and Stimson formations at Marias Pass, Gale crater, Mars, *47th Lunar and Planetary Science Conference*, *47*, 2397.

Ramseyer, K., J. E. Amthor, A. Matter, T. Pettke, M. Wille, and A. E. Fallick (2013), Primary silica precipitate at the Precambrian/Cambrian boundary in the South Oman Salt Basin, Sultanate of Oman, *Mar. Pet. Geol.*, *39*(1), 187–197, doi:10.1016/j.marpetgeo.2012.08.006.

Rapin, W., et al. (2016), Hydration state of calcium sulfates in Gale crater, Mars: Identification of bassanite veins, *Earth Planet. Sci. Lett.*, *452*, 197–205, doi:10.1016/j.epsl.2016.07.045.

Rieder, R., R. Gellert, J. Brückner, G. Klingelhöfer, G. Dreibus, A. S. Yen, and S. W. Squyres (2003), The new Athena alpha particle X-ray spectrometer for the Mars Exploration Rovers, *J. Geophys. Res.*, *108*(E), 8066, doi:10.1029/2003JE002150.

Ruff, S. W., and J. D. Farmer (2016), Silica deposits on Mars with features resembling hot spring biosignatures at El Tatio in Chile, *Nat. Commun.*, *7*, 13,554, doi:10.1038/ncomms13554.

Squyres, S. W., et al. (2008), Detection of silica-rich deposits on Mars, *Science*, *320*(5879), 1063–1067, doi:10.1126/science.1155429.

Stefánsson, A., S. R. Gíslason, and S. Arnórsson (2001), Dissolution of primary minerals in natural waters, *Chem. Geol.*, *172*(3–4), 251–276, doi:10.1016/S0009-2541(00)00262-X.

Thiry, M., A. Milnes, and M. Ben Brahim (2015), Pleistocene cold climate groundwater silicification, Jbel Ghassoul region, Missour Basin, Morocco, *J. Geol. Soc.*, *172*, 125–137, doi:10.1144/jgs2014-033.

Thomson, B. J., N. T. Bridges, R. Milliken, A. Baldridge, S. J. Hook, J. K. Crowley, G. M. Marion, C. R. de Souza Filho, A. J. Brown, and C. M. Weitz (2011), Constraints on the origin and evolution of the layered mound in Gale crater, Mars using Mars Reconnaissance Orbiter data, *Icarus*, *214*(2), 413–432, doi:10.1016/j.icarus.2011.05.002.

Vagle, G. B., A. Hurst, and H. Dypvik (1994), Origin of quartz cements in some sandstones from the Jurassic of the Inner Moray Firth (UK), *Sedimentology*, *41*, 363–377, doi:10.1111/j.1365-3091.1994.tb01411.x.

Vaniman, D. T., et al. (2014), Mineralogy of a mudstone at Yellowknife Bay, Gale crater, Mars, *Science*, *343*(6169), 1243480, doi:10.1126/science.1243480.

Watkins, J. A., et al. (2016), Paleotopography of erosional unconformity, base of Stimson formation, Gale crater, Mars, *47th Lunar and Planterary Science Conference, 47*, p. 2939.

Wiens, R. C., et al. (2012), The ChemCam instrument suite on the Mars Science Laboratory (MSL) rover: Body unit and combined system tests, *Space Sci. Rev.*, *170*(1–4), 167–227, doi:10.1007/s11214-012-9902-4.

Wiens, R. C., et al. (2013), Pre-flight calibration and initial data processing for the ChemCam laser-induced breakdown spectroscopy instrument on the Mars Science Laboratory rover, *Spectrochim. Acta, Part B*, *82*, 1–27, doi:10.1016/j.sab.2013.02.003.

Williams, L. A., and D. A. Crerar (1985), Silica diagenesis, II. General mechanisms, *J. Sediment. Petrol.*, *55*(3), 301–311.

Williams, R. M. E., et al. (2013), Martian fluvial conglomerates at Gale crater, *Science*, *340*(6), 1068–1072, doi:10.1126/science.1237317.

Yen, A. S., et al. (2017), Multiple stages of aqueous alteration along fractures in mudstone and sandstone strata in Gale Crater, Mars, *Earth Planet. Sci. Lett.*, doi:10.1016/k.epsl.2017.04.033, in press.

Erratum

In the originally published version of this article, B. L. Ehlmann was incorrectly listed as co-author. She is now listed in the acknowledgements, and the current version may be considered the authoritative version of record.